Supercritical fluid extraction of essential oil from chamomile seeds: experiments, modelling, and parameter estimation

Oliwer Sliczniuk^{a,*}, Pekka Oinas^{a}

^{a}*Aalto University, School of Chemical Engineering, Espoo, 02150, Finland*

ARTICLE INFO

ABSTRACT

This study investigated the supercritical extraction process of chamomile oil from chamomile seeds. A distributed-parameter model describes the fluid-solid extraction process. The concept of quasi-one-dimensional flow is applied to reduce the number of spatial dimensions. The flow is assumed to be uniform across any cross-section, although the area available for the fluid phase can vary along the extractor. The physical properties of the solvent are estimated from the Peng-Robinson equation of state. Key model parameters included partition factor internal and axial diffusion coefficients were determined using maximum likelihood estimation from experimental data, assuming normal error. A set of laboratory experiments was performed in under multiple constant operating conditions: $30 - 40\,°C$, $100 - 200$ bar, and $1.33 - 6.66 \times 10^{-5}$ kg/s.

1. Introduction

The present study focuses on extracting essential oil from the caraway (Carum carvi L.) seeds with supercritical fluid extraction and modelling that process. Caraway is a biennial plant belonging to the Apiaceae family. It is widespread in Asia, Europe, and North Africa. The essential oil obtained from caraway finds its potential application as a fragrance ingredient in perfumes, liquors, and toothpaste. As presented by Hromis et al. [1], the dried caraway contains nearly 2.8–5% essential oil, from which the main compounds are carvone, pinene, camphene, limonene, and carveol.

The economic feasibility of the process is crucial when selecting the appropriate technology. Conventional processes, such as distillation and organic solvent extraction, are frequently used for essential oil extraction. The distillation process is carried out at a high temperature, which causes thermal degradation of thermolabile compounds—considering that alternative techniques like supercritical fluid extraction gained popularity for extraction. Supercritical carbon dioxide, in particular, is attractive due to its unique properties such as inflammable, non-toxic, low critical temperature and non-corrosive. Furthermore, its critical point is relatively low compared to other fluids, making it a suitable alternative to traditional extraction techniques. The supercritical fluids exhibit both gas- and liquid-like properties so that operating conditions can adjust the dissolving power.

Various mathematical models have been proposed to describe the extraction of valuable compounds from a fixed biomass bed. However, selecting an appropriate extraction model requires understanding the physical phenomena occurring in the operational unit. Each model has its own set of assumptions and describes different mass transfer mechanisms and equilibrium relationships.

One model proposed by Reverchon et al. [2] is the hot ball model, which is based on an analogy to heat transfer and describes an extraction process from solid particles containing small quantities of solute where solubility is not a limiting factor.

Another model, the Broken-and-Intact Cell model, was presented by Sovova [3]. This model describes a system where the outer surfaces of particles have been mechanically interrupted, allowing easy access of solvent to the solute from the broken cells. In contrast, the solute from the intact cells is less accessible due to high mass transfer resistance.

Reverchon [4] developed a model for fluid-solid extraction, where the oil is treated as a single component, and the extraction process is controlled by internal mass transfer resistance, neglecting external mass transfer. However, this model does not consider the influence of axial dispersion or changes in fluid density and flow rate along the bed.

In this work, the fundamental governing equations are derived and combined with the kinetic model suggested by Reverchon [4] to obtain a general model for the oil extraction process from the caraway seed. This model simplifies some of the physical behaviour to obtain a control-oriented model. It is assumed that the extraction process operates semi-continuously in a cylindrical vessel. The solvent is first brought to supercritical conditions, pumped through a fixed bed of finely chopped biomass, and the solute is extracted from the biomass. The solvent and solute are then separated in a flush drum, and the extract is collected. The feed flow rate (F_{in}) and inlet temperature (T_{in}) of the extractor can be measured and manipulated, while the vessel pressure (P) can also be measured and manipulated. However, the outlet temperature (T_{out}) can only be measured. Figure 1 shows a simplified flow diagram.

This study aims to develop a process model for extracting natural substances from solid materials and liquids using supercritical fluids, specifically supercritical CO_2. To achieve this, the solvent properties are estimated based on

*Corresponding author

✉ oliwer.sliczniuk@aalto.fi (O. Sliczniuk)
ORCID(s): 0000-0003-2593-5956 (O. Sliczniuk); 0000-0002-0183-5558 (P. Oinas)
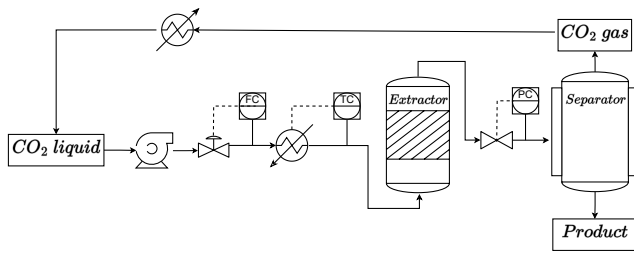
Figure 1: Process flow diagram

thermodynamic relations and the extraction kinetic parameters estimated based on a set of experiments conducted at various conditions. The maximum likelihood estimator is used to solve the parameter estimation problem, and the obtained parameters are subjected to regression to derive correlations. These correlations enable the process model to be generalized across a range of temperatures (40 to 50 °C) and pressures (200 to 300 bar).

The study is structured as follows: Chapter 2.1 provides a general discussion on supercritical fluids to familiarize the reader with their properties. Chapter 2.2 introduces the general balance equations. The balance equations are combined with the extraction kinetic equation to develop the process model in Chapter 2.3. The maximum likelihood technique is presented in Chapter 2.4 and is then combined with the process model. Chapter 2.5 describes the experimental work and the data collected from experiments, which are used to estimate missing parameters related to the extraction kinetic. Finally, the parameter estimations and simulation results are discussed in Chapters 3 and 4

2. Materials and methods

2.1. Supercritical fluids

A supercritical fluid (SCF) is a substance at a temperature and pressure above its critical point, where there are no distinct liquid and gas phases but below the pressure required to compress it into a solid. SCFs can move through porous solids like gases, which is faster than liquid transport through such materials. SCFs have a higher ability to dissolve materials like liquids or solids compared to gases. Near the critical point, small changes in pressure or temperature result in significant changes in density, allowing many properties of an SCF to be fine-tuned. By changing the pressure and temperature, the properties of carbon dioxide can be tuned to be more liquid-like or gas-like.

Fluid properties can be divided into two kinds: equilibrium properties and transport properties. The equation of state can be used accurately to predict the equilibrium properties, such as fluid density, enthalpy, vapour pressure, fugacity and fugacity coefficient, vapour-liquid equilibrium, and all kinds of excess properties.

Supercritical CO_2's thermodynamic properties, such as density or specific heat capacity, vary significantly with slight changes in temperature and pressure due to real gas effects. The Peng-Robinson equation of state (P-R EOS) is

used to calculate the thermodynamic properties by accounting for these real gas effects are presented in Appendix A.1.1. The P-R EOS belongs to a specific class of thermodynamic models for modelling the pressure of a solvent as a function of temperature and density and which can be rewritten as a cubic function of the molar volume.

To determine the thermodynamic properties of a real gas, it is necessary to evaluate the departure function of the chosen equation of state for that property. As explained by Elliott [5], the departure function describe the difference between the actual value of a thermodynamic property of a real gas and its value if the gas were ideal under the same temperature and pressure conditions. The ideal gas serves as a reference state to which the properties of real gases are compared. The departure function measures the extent to which a real gas deviates from ideal gas behaviour. The departure functions allow for the accurate calculation of thermodynamic properties for real gases.

The properties of CO_2 are presented as a function of operating conditions (temperature and pressure) in Figure 2. At standard atmospheric pressure and temperature, CO_2 behaves as an ideal gas, and its compressibility factor equals unity. However, at high pressures and/or low temperatures, intermolecular forces between gas molecules become more significant, causing them to deviate from ideal behaviour. As a result, the compressibility factor can be greater than or less than unity, depending on the magnitude of these forces. As presented in Figure 2a, the compressibility factor obtained from the Peng-Robinson equation of state varies strongly depending on the operating conditions.

The real gas effects are also visible on the density plot presented in Figure 2b. The density calculations are based on the compressibility factor, and its value depends on the operating conditions. The fluid properties near the critical point are unique and combine gas-like and liquid-like properties. The details of calculations are explained in Appendix A.1.2.

Figure 2c show the behaviour of the heat capacity of a supercritical fluid at constant pressure (C_p). The details of the calculations can be found in Appendix A.1.3. Contrary to the density, which varies monotonically, the specific heat shows very high levels in a narrow region. In the subcritical region, the phase transition is associated with an effective spike in the heat capacity (i.e., the latent heat). Approaching the critical point, the latent heat falls to zero, which is accompanied by a gradual rise in heat capacity in the pure phases near phase transition. At the critical point, the latent heat is zero, but the heat capacity shows a diverging singularity. Beyond the critical point, there is no divergence, but rather a peak in the heat capacity; the highest point of this peak identifies the Widom line (as discussed by Simeoni et al. [6] and Banuti [7]).

Figure 2d represent how the specific enthalpy change with the operating conditions. The details of calculations are discussed in Appendix A.1.4.

Transport properties such as viscosity and conductivity play a crucial role in engineering design for production, fluid
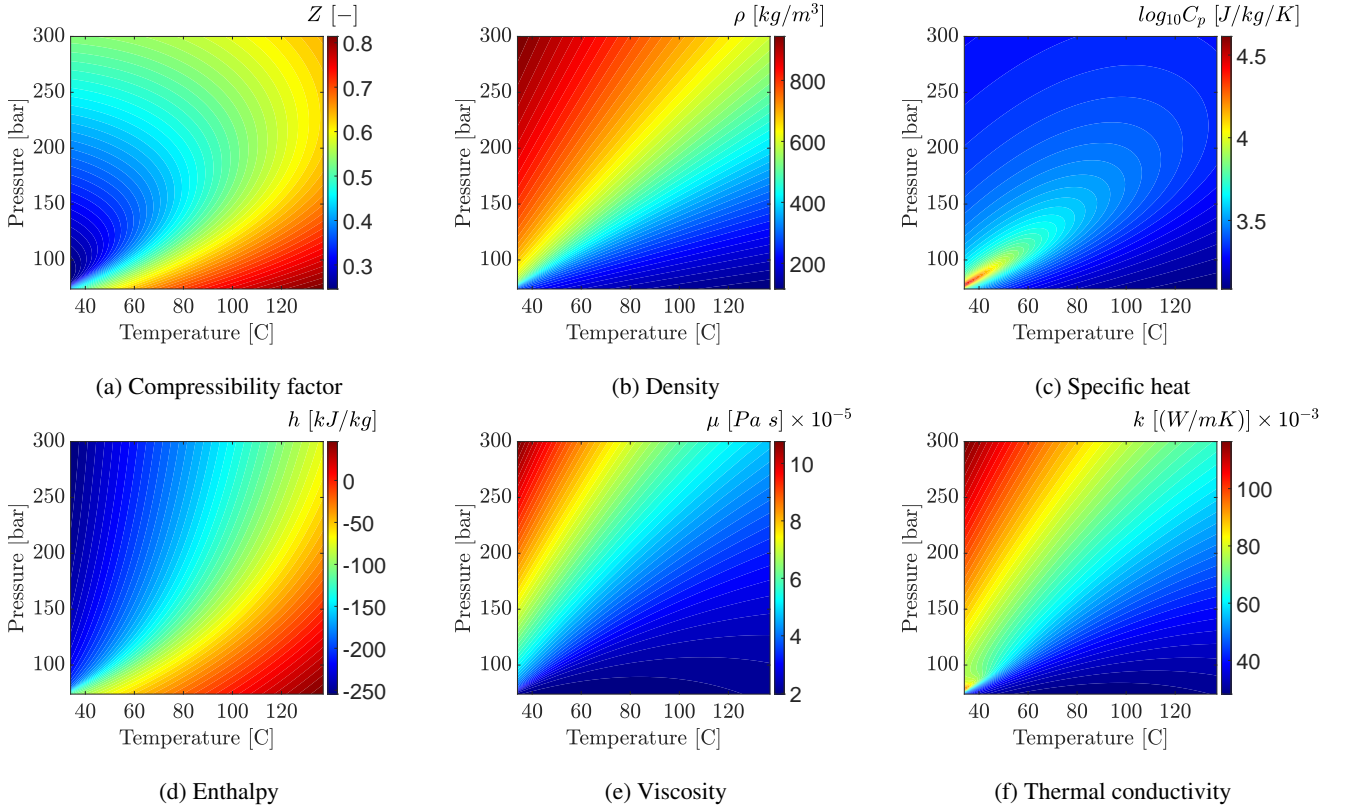
(a) Compressibility factor

(b) Density

(c) Specific heat

(d) Enthalpy

(e) Viscosity

(f) Thermal conductivity

Figure 2: Properties of CO_2 based on the equation of state and correlations

transportation, and processing. However, as highlighted by Sheng et al. [8], developing a satisfactory theory for transport properties of real dense gases and liquids is a challenging task. This is due to the inherent difficulties involved in accurate measurements and the complexity involved in theoretical treatments.

To address this issue, the correlations of transport coefficients are either empirical or based on some theoretical foundation. Chapman-Enskog's theory (presented in Chapman and Cowling [9]) for transport properties of dense gases based on the distribution function is a popular theoretical approach. However, the Chapman-Enskog theory was developed for rigid spherical molecules and modifications are required to apply it to real gases. Many correlations have been proposed following the Chapman-Enskog theory in the form of reduced density and reduced temperature, such as those developed by Fenghour et al. [10], and Laesecke and Muzny [11] from the National Institute of Standards and Technology (NIST). The correlation of Laesecke and Muzny [11] is presented in Figure 2e.

NIST has developed a viscosity formulation consisting of four contributions: (i) for the limit of zero density, (ii) for the initial density dependence, (iii) for the residual viscosity, and (iv) for the singularity of the viscosity at the critical point. The NIST correlation covers temperatures from 100 to 2000 K for gaseous CO_2, and from 220 to 700 K with pressures along the melting line up to 8000 MPa for compressed and supercritical liquid states. These correlations

and theories are essential in predicting transport properties for real gases and liquids and can assist in engineering design and analysis.

Similarly, the NIST developed the correlation, which describe the behaviour of thermal diffusivity of CO_2. The work of Huber et al. [12] captures the singular behaviour of thermal conductivity around the critical point. The correlation is applicable for the temperature range from the triple point to 1100 K and pressures up to 200 MPa. Figure 2f shows how the thermal conductivity of carbon dioxide change depending on the operating conditions.

2.2. Governing equations

The governing equation for a quasi-one-dimensional compressible flow in Cartesian coordinates can be found in the Appendix A.2 and in the work of Anderson [13]. Quasi-one-dimensional flow is a fluid flow characterized by the assumption that the flow properties remain uniform across any given cross-section of the flow. This assumption is made when there is a variation in the cross-sectional area of the flow channel, such as an irregular shape or partial filling of an extractor. In such cases, the flow is considered to be quasi-one-dimensional because the velocity and other flow properties are assumed to vary only in the direction of flow.

The quasi-one-dimensional compressible Navier-Stokes equations in Cartesian coordinates are given by Equations 1 to 3. The derivation of these Equations are presented in Appendix A.2.

$$\frac{\partial \left(\rho_f A_f(z) \right)}{\partial t} + \frac{\partial \left(\rho_f A_f(z) v \right)}{\partial z} = 0 \tag{1}$$

$$\frac{\partial \left(\rho_f v A_f(z) \right)}{\partial t} + \frac{\partial \left(\rho_f A_f(z) v^2 \right)}{\partial z} = -A_f(z) \frac{\partial P}{\partial z} \tag{2}$$

$$\frac{\partial \left(\rho_f e A_f(z) \right)}{\partial t} + \frac{\partial \left(\rho_f A_f(z) v e \right)}{\partial z} = -P \frac{\left(A_f(z) v \right)}{\partial z} + \frac{\partial}{\partial z} \left(\frac{\partial T}{\partial z} \right) \tag{3}$$

where ρ_f is the density of the fluid, $A_f(z)$ is the function which describe change of the cross-section, v is the velocity, P is the total pressure, e is the internal energy of the fluid, t is time and z is the spacial direction.

Based on governing equations, the small discontinuity (defined as δ) in flow properties, shown in Figure 3, can be analysed. The analysis follows the work of Schreier [14].

	ρ_f	$\rho_f + \delta \rho_f$	
$v \rightarrow$	P	$P + \delta P$	$v + \delta v \rightarrow$
	T	$T + \delta T$	

Figure 3: Small discontinuity in one-dimensional flow

The discontinuity is presumed to be at rest relative, and the balance equations become

$$\rho_f \delta v + v \delta \rho_f + \delta \rho_f \delta v = 0$$

$$\delta P = \delta v \delta \rho_f$$

These relations are equally valid if the two regions are separated by a region of finite width rather than a discontinuity.

$$\lim_{\rho_f v \to 0} \rho_f \delta v + v \delta \rho_f + \delta \rho_f \delta v = 0 / \delta \rho_f \rightarrow \frac{dv}{d\rho_f} = -\frac{v}{\rho_f}$$

By combining the momentum equation with the above equation, we get

$$\frac{dv}{d\rho_f} = -\frac{dv}{dP}\frac{dP}{d\rho_f} = -\frac{1}{\rho v}\frac{dP}{d\rho_f} = -\frac{v}{\rho_f} \tag{4}$$

Suppose the flow is presumed to be isentropic, $dP/d\rho_f = c^2$, so $v^2 = c^2$, where c is the speed of sound. This can be interpreted as a small pressure wave propagating with the speed of sound relative to the flow. Moreover, if the flow velocity is relatively low, all pressure changes are hydrodynamic (due to velocity motion) rather than thermodynamic which leads to $\partial \rho_f / \partial P \approx 0$. In other words, the small changes in pressure due to flow velocity changes do not change the density.

2.3. Extraction model
2.3.1. Continuity equation
The obtained above quasi-one-dimensional continuity equation (Equation 1) is further modified by specifying a function $A_f(z) = A\phi(z)$ to take into account the change of the cross-section available for the fluid. The Equation 5 shows the differential form of the continuity equation:

$$\frac{\partial(\rho_f(T(t,z), P(t))\phi(z))}{\partial t} + \frac{\partial(\rho_f(T(t,z), P(t))v A\phi(z))}{\partial z} = 0 \tag{5}$$

where A is the total cross-section of the extractor and $\phi(z)$ describe porosity along the extractor.

Assuming that the mass flow rate is constant in time, the temporal derivative becomes zero, and the spatial derivative can be integrated along z as

$$\int \frac{\partial(\rho_f(T(t,z), P(t))v A\phi(z))}{\partial z} dz = 0 \rightarrow F = \rho_f(T(t,z), P(t))v A\phi(z) \tag{6}$$

Here, F is a constant obtained from the integration and is understood as the mass flux per unit area, which is assumed to be constant along z. To simplify the dynamics of the system, it is assumed that $F = F(t)$ is a control variable and affects the whole system instantaneously. This assumption allows for finding the velocity profile that satisfies mass continuity based on $F(t)$, $\phi(z)$, and $\rho_f(T(t,z), P(t))$.

$$v = \frac{F(t)}{\rho_f(T(t,z), P(t)) A\phi(z)} \tag{7}$$

The fluid density $\rho_f(T(t,z), P(t))$ can be obtained from an equation of state if temperature and the thermodynamic pressure (assumed $P(t)$ to be constant along z due to the low-Mach number condition) are known. The variation in density may be caused by the fluid accumulation in the system (equivalent to pressure change), which occurs instantaneously along z or by a temperature change.

Analogously, the superficial velocity might be introduced to the model and defined as

$$u = v\phi(z) = \frac{F(t)}{\rho_f(T(t,z), P(t)) A} \tag{8}$$

2.3.2. Mass balance for the fluid phase
The detailed derivation of the mass balance equation for the fluid phase can be found in Appendix A.2. The movement of the pseudo-homogeneous fluid phase (Equation 9) is considered only in the axial direction due to quasi-one-dimensional assumptions, which take into account variation of the void fraction. Furthermore, the thermodynamic pressure is assumed to be constant along the device as presented by Equation 4. Additionally, the boundary layer adjacent to the inner wall of the extractor is neglected, resulting in a constant velocity profile across any cross-section of the extractor perpendicular to the axial direction. The amount of solute in the solvent is considered negligible, resulting in the fluid phase being described as pseudo-homogeneous, and its properties are assumed to be the same as the solvent. The mass balance equation for the fluid phase includes convection, diffusion, and kinetic terms.

$$\frac{\partial c_f(t,z)}{\partial t} + \frac{1}{\phi(z)} \frac{\partial \left(c_f(t,z) u \right)}{\partial z} = \frac{1-\phi(z)}{\phi(z)} r_e(t,z) + \frac{1}{\phi(z)} \frac{\partial}{\partial z} \left(D_e^M \frac{\partial c_f(t,z)}{\partial z} \right) \tag{9}$$

$c_f(t,z)$ represents the concentration of solute in the fluid phase, , $r_e(t,z)$ is a mass transfer kinetic term, and $D_e^M(T(t,z), P(t), F(t))$ is the axial mass diffusion coefficient.

2.3.3. Mass balance for the solid phase

The solid phase is considered to be stationary, with negligible convection and diffusion terms in the mass balance equation (Equation 10). Therefore, the only significant term in this equation is the kinetic term (as defined in Equation 11), which connects the solid and fluid phases. The extract is represented by a single pseudo-component to simplify the analysis.

$$\frac{\partial c_s(t, z)}{\partial t} = \underbrace{r_e(t, z)}_{\text{Kinetics}} \tag{10}$$

2.3.4. Kinetic term

The kinetic term in this study is based on the two-film theory proposed by Reverchon [4], and the mass transfer kinetic is given by Equation 11. This equation takes into account the overall diffusion coefficient and the concentration gradient, which acts as the driving force for the process.

As the solvent flows through the bed, CO_2 molecules diffuse into the pores and adsorb on the particle surface to form an external fluid film around the solid particles due to the solvent-solid matrix interactions. The effect of Knudsen diffusion is negligible in this process, as the mean free path of the molecule is much smaller than the pore diameter. The dissolved solute diffuses from the particle's core through the solid-fluid interface, the pore, and the film into the bulk. Figure 4 illustrates the mass transfer mechanism, where the mean solute concentration in the solid phase is denoted as c_s and the equilibrium concentrations at the solid-fluid interface are denoted as c_s^* and c_p^*, respectively, for solid and fluid phases. The concentration of the solutes in the fluid phase in the center of the pore is denoted as c_p. As the solute diffuses through the pore, its concentration changes and reaches c_{pf} at the opening of the pore. The solute then diffuses through the film around the particle and reaches a concentration in bulk c_f. The two-film theory describes the solid-fluid interface inside the pore. The overall mass transfer coefficient can be determined if the relationship between the solute concentration in one phase and its equilibrium concentration is known.

Bulley et al. [15] suggests a process where the driving force for extraction is given by the difference between the concentration of the solute in bulk, c_f, and in the center of the pore, c_p^*. The concentration c_p^* is in equilibrium with c_s according to an equilibrium relationship. The rate of extraction is thus $r_e\left(c_f - c_p^*(c_s)\right)$.

On the other hand, Reverchon [4] proposes a driving force given by the difference between c_s and c_p^*. c_p^* is determined by an equilibrium relationship with c_f and the extraction rate is $r_e\left(c_s - c_p^*(c_f)\right)$ or more precisely

$$r_e(t, z) = \frac{D_i(T(t, z), P(t))}{\mu l^2}\left(c_s(t, z) - c_P^*(t, z)\right) \tag{11}$$

where μ is sphericity, l a characteristic dimension of particles and can be defined as $l = r/3$, r is the mean particle radius, ρ_s is the solid density, $D_i(T(t, z))$ corresponds to the overall diffusion coefficient and $c_P^*(t, z)$ is a concentration
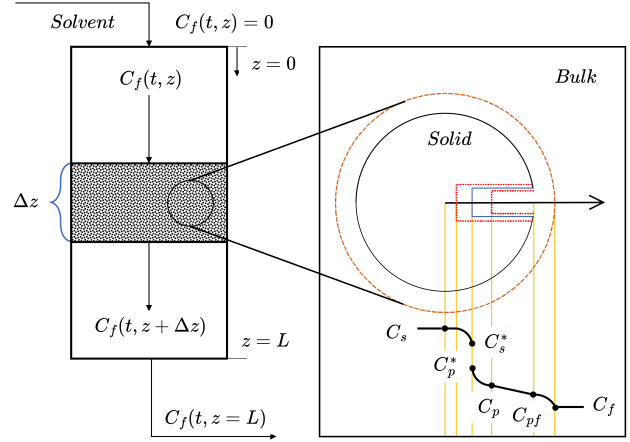

Figure 4: The extraction mechanism

at the solid-fluid interface (which according to the internal resistance model is supposed to be at equilibrium with the fluid phase).

According to Bulley et al. [15], a linear equilibrium relationship (equation 12) can be used to find an equilibrium concentration of the solute in the fluid phase $c_f^*(t, z)$ is based on the concentration of the solute in the solid phase $c_s(t, z)$

$$c(t, z) = k_p(T(t, z), P(t))q^*(t, z) \tag{12}$$

The volumetric partition coefficient $k_p(T(t, z), P(t))$ behaves as an equilibrium constant between the solute concentration in one phase and the corresponding equilibrium concentration at the solid-fluid interphase. According to Spiro and Kandiah [16], the term $k_p(T(t, z), P(t))$ can be expressed as the function of mass partition factor $k_m(T(t, z))$.

$$k_m(T(t, z)) = \frac{k_p(T(t, z), P(t))\rho_s}{\rho(T(t, z), P(t))} \tag{13}$$

Equation 14 represents of the kinetic term according to Reverchon [4]

$$r_e(t, z) = -\frac{D_i(T(t, z), P(t))}{\mu l^2}\left(c_s(t, z) - \frac{\rho_s}{k_m(T(t, z))\rho_f(T(t, z), P(t))}c_f(t, z)\right) \tag{14}$$

2.3.5. Uneven distribution of the solute in the solid phase

Following the idea of the Broken-and-Intact Cell (BIC) model presented by Sovova [17], the internal diffusion coefficient D_i is consider to be a product of the reference value of D_i^R and the exponential decay function γ, as given by Equation 15.

$$D_i = D_i^R\gamma(c_s(t, z)) = D_i^R \exp\left(\Upsilon\left(1 - \frac{c_s(t, z)}{c_{s0}}\right)\right) \tag{15}$$

where the Υ describe the curvature of the decay function. The final form of the extraction kinetic Equation is given by Equation 16.

$$r_e(t, z) = -\frac{D_i^R(T(t, z), P(t))\gamma(c_s(t, z))}{\mu l^2}\left(c_s(t, z) - \frac{\rho_s}{k_m(T(t, z))\rho(T(t, z), P(t))}c_f(t, z)\right)$$

(16)

Such a formulation limits the availability of the solute in the solid phase. Similarly to the BIC model, if solute is assumed to be contained in the cells, a part of which is open because the cell walls were broken by grinding, and the rest remains intact. The diffusion of the solute from a particle's core takes more time compared to the diffusion of the solute located close to the outer surface. Considering that the internal diffusion coefficient decay as the concentration of the solute in the solid decrease. As the value of the c_s decrease over time, the exponential term approach unity and $\lim_{c_s \to 0} D_i = D_i^R$. D_i^R can be interpreted as the internal diffusion coefficient at vanishing gradient.

Alternatively, the decay function γ can be consider with respect to the Shrinking Core model presented by Goto et al. [18], where the particle radius change as the amount of solute in the solid phase decrease. As the particle size decrease due to dissolution, the diffusion path increase which makes the diffusion slower and reduce the value of a diffusion coefficient. The same analogy can be apply to the Equation 15 to explain the change of the diffusion coefficient.

2.3.6. Heat balance

The heat governing equation describe the evolution of the energy in the system and it is given by 17. The derivation of the heat equation can be found in Appendix A.2.

$$\frac{\partial \left(\rho_f(T(t,z), P(t)) e(t,z) A_f \right)}{\partial t} + \frac{\partial \left(\rho_f(T(t,z), P(t)) A_f v e(t,z) \right)}{\partial z}$$
$$= -P(t) \frac{(A_f v)}{\partial z} + \frac{\partial}{\partial z} \left(\frac{\partial T(t,z)}{\partial z} \right) \quad (17)$$

The departure function is a mathematical function that characterizes the deviation of a thermodynamic property (enthalpy, entropy, and internal energy) of a real substance from that of an ideal gas at the same temperature and pressure. The departure function is typically defined as the difference between the value of a thermodynamic property for a real fluid and the corresponding value for an ideal gas at the same temperature and pressure. They are typically computed by integrating a function that depends on the equation of state and its derivatives. Following Elliott [5] or Gmehling et al. [19], a real gas internal energy definition can be obtained from the departure functions, defined through Equation 18. More information on the departure functions can be found in Appendix A.1.4.

$$de(t,z) = C_v dT - \left[P(t) - T(t,z) \left(\frac{\partial P(t)}{\partial T(t,z)} \right)_{v_m(T(t,z), P(t))} \right] dv_m(T(t,z), P(t)) \quad (18)$$

where $e^{id}(t,z)$ is the internal energy of perfect gas.

Suppose a gas is considered to be perfectly caloric ($e(t,z) = C_v T(t,z)$), then the energy equation can be written explicitly in the form of temperature. The perfectly caloric gas can be seen as the special case of a real gas, where the second term of Equation 18 goes to zero and the heat capacity C_v is constant.

For real gases, it is complicated to write the heat balance in terms of temperature, but it be can be used directly in the form of internal energy, as it is given by Equation 3. In such a case, the temperature needs to be recovered from the internal energy. A relation for the internal energy can be obtained from an equation of state. For Peng-Robinson, such a relation is given by Equation 19 as presented by Elliott [5].

$$\frac{e(t,z) - e^{id}(t,z)}{RT(t,z)} =$$
$$-\frac{A(T(t,z), P(t))}{B(T(t,z), P(t))} \frac{\kappa \sqrt{T_r}}{\sqrt{8}} \frac{1}{\sqrt{\alpha}} \ln \left[\frac{Z(T(t,z), P(t)) + \left(1 + \sqrt{2}\right) B(T(t,z), P(t))}{Z(T(t,z), P(t)) + \left(1 - \sqrt{2}\right) B(T(t,z), P(t))} \right]$$
(19)

To solve Equation 19, temperature, pressure, and density values need to be known. If an equation of state is introduced, then only two out of three variables need to be obtained as the third one can be calculated; this can be represented as follow

$$e(t,z) = e(T(t,z), P(t), \rho_f(T(t,z), P(t))) = e(T(t,z), P(t), \rho_f(T(t,z), P(t))) \quad (20)$$

If the value of internal energy $e(t,z)$ is known from the time evolution of the energy Equation 3, and pressure is known from measurement, then the temperature can be reconstructed. A rootfinder can be used to find a value of temperature, which minimizes the difference between the value of internal energy coming from the time evolution (Equation 17) and the output from Equation 19. Such a procedure allow to find local temperature along spatial direction z and needs to be repeated every time-step.

Another way to express the energy equation is to introduce enthalpy $h(t,z) = e(t,z) + P(t)/\rho_f(T(t,z), P(t))$. By introducing the definition of enthalpy, the energy equation becomes

$$\frac{\partial \left(\rho_f(T(t,z), P(t)) h(t,z) A_f \right)}{\partial t} = -\frac{\partial \left(\rho_f(T(t,z), P(t)) h(t,z) A_f v \right)}{\partial z}$$
$$+ \frac{\partial \left(P(t) A_f \right)}{\partial t} + \frac{\partial}{\partial z} \left(k \frac{\partial T(t,z)}{\partial z} \right)$$
(21)

The main advantage of this formulation is the presence of term $\partial P(t)/\partial t$, which allows it to directly affect the system through the change of thermodynamic pressure (which is a control variable). The enthalpy is related to the pressure and temperature through the following equation:

$$h(t,z) = h(T(t,z), P(t), \rho_f(T(t,z), P(t))) = h(T(t,z), P(t), \rho_f(T(t,z), P(t))) \quad (22)$$

If the value of enthalpy is known from the time evolution and pressure can be measured, then the Equation 22 can be solved for the temperature to recover the temperature profile. For the Peng-Robinson EoS, the enthalpy can be defined by Equation 23. More details can be found in Appendix A.1.4 or given by Gmehling et al. [19].

$$h(t,z) - h(t,z)^{id} = RT(t,z) \left[T_r(Z(T(t,z), P(t)) - 1) \right.$$
$$-2.078(1 + \kappa) \sqrt{\alpha(T(t,z))} \ln \left(\frac{Z(T(t,z), P(t)) + \left(1 + \sqrt{2}\right) B(T(t,z), P(t))}{Z(T(t,z), P(t)) + \left(1 - \sqrt{2}\right) B(T(t,z), P(t))} \right) \right] \quad (23)$$

The Equation 23 requires an reference sate, which in this case is assumed to be $T_{ref} = 298.15$ [K] and $P_{ref} = 1.01325$ [bar].

As discussed by Gmehling et al. [19], the influence of the intermolecular forces on the enthalpy is needs to taken into account in high pressures systems. In most cases, these forces are attractive, so additional energy is necessary to move the molecules away from each other, that is, to lower the density. If this energy is not added, the substance cools down when it is expanded.

2.3.7. Pressure term

The pressure term in the energy equation, given by Equation 21, describes the change of the thermodynamic pressure with respect to time. As explained in Chapters 2.2, at Low-Mach number conditions, the thermodynamic pressure is nearly constant in space due to the small pressure wave propagation that occurs at the speed of sound. Under such conditions, the term $\partial P/\partial t$ can be approximated by an ordinary differential equation, which describes the instantaneous change of pressure in the system. The pressure (P) in the system is considered a state variable, while the pressure in the new time-step (P_{in}) is considered a control variable.

$$\frac{\partial P(t)}{\partial t} \approx \frac{P(t) - P_{in}(t)}{\Delta t} \tag{24}$$

Such a simplified equation takes into account the pressure change in the energy balance, but the dynamics are simplified and do not consider the effects of pressure losses. In a real system, the dynamics of pressure change would depend on a pump used in an extraction system, as well as a back-pressure regulator used to control an outlet valve.

2.3.8. Extraction yield

The efficiency of the process (the yield) is calculated according to Equation 25 as presented by Sovova et al. [20]. The measurement equation evaluate the mass of solute at the outlet of the extraction unit and sums it. The integral form of the measurement equation (25) can be transformed into the differential form (26) and augmented with the process model.

$$y(t) = \int_{t_0}^{t_f} \frac{F(t)}{\rho_f(T(t,z), P(t))} c_f(t,z) \Big|_{z=L} dt \tag{25}$$

$$\frac{dy(t)}{dt} = \frac{F(t)}{\rho_f(T(t,z), P(t))} c_f(t,z) \Big|_{z=L} \tag{26}$$

2.3.9. Initial and boundary conditions

It is assumed that the solvent is free of solute at the entrance of the extractor and that all the solid particles have the same initial solute content c_{s0}. As the residence time is much shorter than the sampling time, the initial state estimate for the concentration of the solute in the fluid phase would be not reliable. Considering that it is assumed that the $c_f 0 = 0$. Moreover, it is considered that the initial temperature of the extractor in every place is the same and described by h_0. Therefore, the initial conditions employed in the simulation are:

$$c_f(t=0, z) = 0 \qquad c_s(t=0, z) = c_{s0} \qquad h(t=0, z) = h_0$$

$$\frac{\partial c_f(t, z=L)}{\partial x} = 0 \qquad c_s(t=0, z) = c_{s0} \qquad \frac{\partial h(t, z=L)}{\partial x} = 0$$

2.3.10. State-space representation

The process model can be written in a general form:

$$\begin{bmatrix} \dfrac{\partial c_f(t,z)}{\partial t} \\ \dfrac{\partial c_s(t,z)}{\partial t} \\ \dfrac{\partial h(t,z)}{\partial t} \\ \dfrac{\partial P(t,z)}{\partial t} \\ \dfrac{\partial y(t)}{\partial t} \end{bmatrix} = \begin{bmatrix} \bar{\phi}_1\left(c_f(t,z), c_s(t,z), h(t,z); \Theta\right) \\ \bar{\phi}_2\left(c_f(t,z), c_s(t,z), h(t,z); \Theta\right) \\ \bar{\phi}_3\left(c_f(t,z), c_s(t,z), h(t,z); \Theta\right) \\ \bar{\phi}_4\left(c_f(t,z), c_s(t,z), h(t,z); \Theta\right) \\ \bar{\phi}_5\left(c_f(t,z), c_s(t,z), h(t,z); \Theta\right) \end{bmatrix} = \bar{\phi}(t,z; \Theta) = \frac{\partial \chi(t,z)}{\partial t}$$

$$\tag{27}$$

where Θ is a paramter space, $\bar{\phi}$ is a set of functions that correspond to state equations of the model, and χ is the state-space model.

Function $\bar{\phi}$ are transformed to a corresponding set of N_z discretized equations denoted as G. The state-space model $\chi(t,z)$ after the discretization is represented by $\dot{x}(t)$.

$$\dot{x}(t) = \frac{dx(t)}{dt} = \begin{bmatrix} \dfrac{dc_{f,1}(t)}{dt} \\ \vdots \\ \dfrac{dc_{f,N_z}(t)}{dt} \\ \dfrac{dc_{s,1}(t)}{dt} \\ \vdots \\ \dfrac{dc_{s,N_z}(t)}{dt} \\ \dfrac{dh_1(t)}{dt} \\ \vdots \\ \dfrac{dh_{N_z}(t)}{dt} \\ \dfrac{dP(t)}{dt} \\ \dfrac{dy(t)}{dt} \end{bmatrix} = \underbrace{\begin{bmatrix} G_1\left(c_f(t), c_s(t), h(t); \Theta\right) \\ \vdots \\ G_{N_z}\left(c_f(t), c_s(t), h(t); \Theta\right) \\ G_{N_z+1}\left(c_f(t), c_s(t), h(t); \Theta\right) \\ \vdots \\ G_{2N_z}\left(c(t), c_s(t), h(t); \Theta\right) \\ G_{2N_z+1}\left(c_f(t), c_s(t), h(t); \Theta\right) \\ \vdots \\ G_{3N_z}\left(c_f(t), c_s(t), h(t); \Theta\right) \\ G_{3N_z+1}\left(c_f(t), c_s(t), h(t); \Theta\right) \\ G_{3N_z+2}\left(c_f(t), c_s(t), h(t); \Theta\right) \end{bmatrix}}_{G(x(t);\Theta)}$$

where $x \in \mathbb{R}^{N_x = 3N_z}$ and $\Theta \in \mathbb{R}^{N_\Theta = N_\theta + N_u}$, N_θ is the number of model parameters, N_u is the number of control variables.

In a state-space sense, the state variables of the system are the local concentrations of solute in the fluid and solid phases ($c_f(t,z)$ and $c_s(t,z)$, respectively), and the local enthalpy of the pseudo-homogeneous phase ($h(t,z)$). The controllable input variables are the mass flow-rate and temperature of the solvent in the feed and the pressure in the extractor. Additionally, the pressure change is augumented with the state-space and denoted as $P(t)$. The system state-space is extended by assuming that extraction yield can be modelled as a function of a known initial mass of solute in

the solid phase and it can be measured after the separator ($Y(t)$). The system is controllable by manipulating the flow-rate and temperature (enthalpy) of CO_2 in the feed, and the pressure in the extractor.

2.3.11. Discretization methods

The method of lines is used to transform the process model equations into a set of ODEs denoted as $G(x(t); \Theta)$. The partial derivatives in z-direction are computed using a first-order and second-order finite difference approximation. The backward finite difference is used to approximate the first-order derivative, while the central difference scheme is used to approximate the second-order derivative. The length of the fixed bed is divided into N_z equally distributed points in z-direction.

As presented in Appendix A.2, all the governing can be written in the integral form using the Divergence Theorem. The integral equation states that the change rate of the integral of any quantity over an arbitrary control volume is given by the flux through the boundary of the control volume, with being the outer surface normal through the boundary. That quantity is neither produced nor consumed inside of the control volume and is hence conserved. For a derivative to be conservative, it must form a telescoping series. In other words, after the addition of all terms coming from the discretization over a grid, only the boundary terms should remain and the artificial interior points should cancel out. To ensure the mass conservation, the discretization is applied on the conservative form of the process model.

2.4. Parameter estimation

Not all the parameters present in a process model can be estimated from the theoretical considerations. The goal of parameter estimation is to obtain the "best" estimate of unknown parameters θ (which is a subset of the parameter space Θ containing all parameters of a model) based on the continuous observations $Y(t)$ or the discrete observations $Y(t_i)$. Conceptually, the unobservable error $\epsilon(t)$ is added to the deterministic model output, $y(t)$ (Equation 25), to give the observable dependent variable $Y(t)$ (for example results of an experiment). For discrete observations, this can be expressed as:

$$Y(t_i) = y(\theta, t_i) + \epsilon(t_i)$$

For continuous variables, the equation is:

$$Y(t) = y(\theta, t) + \epsilon(t)$$

However, obtaining analytical solutions for a deterministic process model can be challenging, so experiments are often conducted where the vector of derivatives $dY(t_i)/dt$ is measured instead of $Y(t_i)$ itself. In such cases, it is assumed that the unobservable error is added to the deterministic derivative $dy(\theta, t_i)/dt$ as shown below

$$\frac{dY(t_i)}{dt} = \frac{dy(\theta, t_i)}{dt} + \epsilon(t_i) \qquad (28)$$

In the case where the error in the first observation is denoted as ϵ_1, the error in the second observation ϵ_2' incorporates ϵ_1 as well as an independent random component, given

by $\epsilon_2' = \epsilon_1 + \epsilon_2$. Similarly, the error in the third observation is $\epsilon_3' = \epsilon_1 + \epsilon_2 + \epsilon_3$, and so on. Mandel [21] made a distinction between the typically assumed independent measurement error in the dependent variable and a "cumulative" or interval error, in which each new observation encompasses the error of the previous ones. Cumulative errors arise from fluctuations in the process itself due to small variations in operating conditions and are not independent; only the differences in measurement from one period to the next are independent.

Maximum likelihood estimation (MLE) is a statistical method used to estimate the parameters of a probability distribution based on observed data. The MLE works by finding the values of the parameters that maximize the likelihood function, which is the probability of observing the given data for a given set of parameter values. The MLE has desirable properties such as asymptotic efficiency and normality. Although the MLE has often been associated with the normal distribution for mathematical convenience, it can be applied to a wide range of probability distributions. The derivation of the likelihood function under the assumption of the Gaussian distribution is presented in Appendix A.4. The final form of the objective function is presented by Equation 29:

$$\ln L = -\frac{n}{2} \ln \sqrt{2\pi\sigma^2} - \frac{\sum_{i=1}^{n} \left[\frac{dY(t_i)}{dt} - \frac{dy(\theta, t_i)}{dt} \right]^2}{2\sigma^2} \qquad (29)$$

The parameter estimation problem can be formulated as follow:

$$
\begin{aligned}
\hat{\theta}_{MLE} &= \arg\max_{\sigma, \theta \in \Theta} \ln L = \arg\max_{\sigma, \theta \in \Theta} p(\theta|y) \\
\text{subject to} \quad & \dot{x} = G(x(t); \theta) \\
& \dot{\theta} = 0 \\
& y = y(t) \\
& \theta^{lb} \le \theta \le \theta^{ub}
\end{aligned}
\qquad (30)
$$

where $\hat{\theta}$ is as maximum likelihood estimator, θ^{lb} define the minimal value of θ and θ^{ub} is the maximum value of θ.

Based on the first order optimality condition, the $\ln L$ can be maximized with respect to the vector θ and equating to zero the partial derivatives of $\ln L$:

$$\frac{\partial \ln L}{\partial \theta} = \frac{\partial \sum_{i=1}^{n} \ln p \left(y(t_i)|\theta \right)}{\partial \theta} = 0 \qquad (31)$$

Solution of Equations 31 yield the desired estimates $\hat{\theta}$. For some models, these equations can be explicitly solved for $\hat{\theta}$ but in general, no closed-form solution to the maximization problem is known or available, and a maximum likelihood estimator can only be found via numerical optimization.

As a result of fitting, the following parameters are obtained:

- Partition coefficient: $\qquad k_m$

- Internal diffusion coefficient: $\quad D_i^R$

- Decay coefficient: $\qquad \Upsilon$

- Standard deviation: $\qquad \sigma^2$

To ensure that parameters found by the optimizer do not reach unrealistic values, an additional set of inequality constraints is introduced. The initial guess for each optimization, the lower and upper bounds for each parameter are given in Table 1.

Parameter	k_m[-]	$D_i^R \times 10^{-13}[m^2/s]$	$D_e^M[m^2/s]$	Υ [m^3/kg]	σ[-]
Lower bound	0	0	0	0	0
Upper bound	$+\infty$	$+\infty$	$+\infty$	$+\infty$	$+\infty$
Initial guesses	0.1-10	$0.1 - 10$	0	0.1-10	0.01

Table 1: Constraints and initial guess

2.5. Experimental work

In order to solve the optimization problem presented by Equation 30, it is necessary to have knowledge of the dataset $Y(t)$, which was obtained by extracting oil from chamomile seeds. The experiments were performed by Povh et al. [22]. To prepare the seeds for extraction, they were first pre-treated using a knife mill (TECNAL, model TE 340) to reduce their particle size. The mean particle diameter was determined by the Sauter equation and is equal to 0.3×10^{-3}m. The actual density of the chamomile particles was measured through helium pycnometry at the Institute of Chemistry IQ/Unicamp's Analytical Facilities. The bulk density of the bed was computed based on the feed's mass and the extractor's volume. The total porosity of the bed, including the particles, was determined using the following calculation: $\epsilon = 1 - \frac{d_a}{d_r} = 1 - \frac{370}{1364} = 0.73$.

The experiments were conducted using an extractor with diameter of 3.96×10^{-2} m and length 16.55×10^{-2} m. Twelve experiments were performed under different but constant in time operating conditions: $30 - 40°C$, $100 - 200$ bar, and $1.33 - 6.66 \times 10^{-5}$ kg/s. The amount of solid material used for extraction was 75×10^{-3} kg, which was sufficient to fill the whole vessel. Samples were collected every 30 min for the first 3 h and every hour afterwards up to 10 h.

3. Results

The parameter estimation problem was solved by fitting the process model to the dataset given in the Figure 5. Each time-series was fitted to the model separately. The blue dots indicate the data point obtained as a measurement from the laboratory experiments. The black curve represents the yield curve obtained from the initial guess of the parameters. The red curve correspond to yield curve obtained as a solution of the optimization problem. Every sub-figure is made of two figure of which one represent the cumulative yield, and the second one shows the derivative of the cumulative yield. As explained in Chapter 2.4, the derivatives of the cumulative measurements are independent on the previous measurement and should be used for the parameter estimation. The parameters obtained from solving the optimization problem can be found in Table 2.

As shown in the Table 2, the optimizer found optimal values of the partition factors k_m at relatively high levels. Such a behaviour suggest that the solvent is far from the
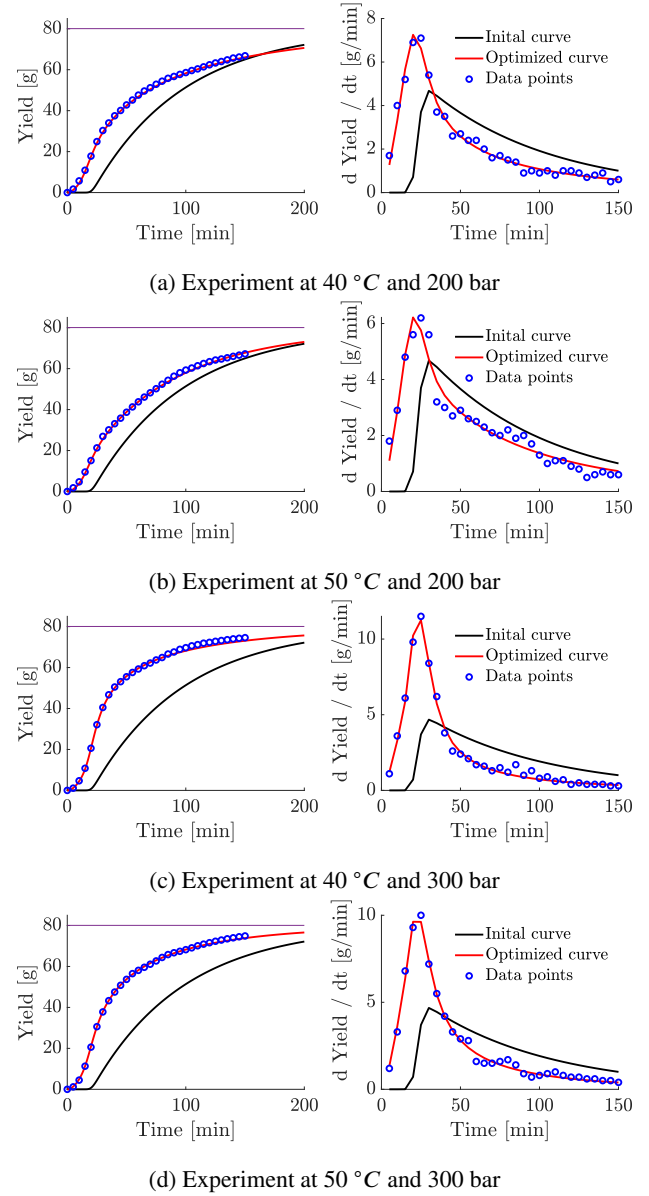

(a) Experiment at 40 °C and 200 bar

(b) Experiment at 50 °C and 200 bar

(c) Experiment at 40 °C and 300 bar

(d) Experiment at 50 °C and 300 bar

Figure 5: Results of parameter estimation

	40 °C 200 *bar*	50 °C 200 *bar*	40 °C 300 *bar*	50 °C 300 *bar*
$k_m[-]$	24254	198335	99496	238448
$D_i[m^2/s] \cdot 10^{-14}$	4.32	3.34	14.39	8.82
$D_e^M[m^2/s] \cdot 10^{-6}$	7.79	7.99	4.16	5.05
$\Upsilon[-]$	1.07	0.29	2.11	1.29
$\tau[-]$	0.72	0.76	0.71	0.69
$\sigma[-]$	0.07	0.12	0.07	0.05

Table 2: Parameter estimation results

saturation, and the model can be simplified. The model reduction can be introduced by considering the limit of the concentration gradient

$$\lim_{k_m \to \infty} \left(c_s(t,z) - \frac{\rho_s}{k_m(T(t,z))\rho(T(t,z),P(t))} c_f(t,z) \right) =$$

$$= \left(c_s(t,z) - \frac{\rho_s}{\infty\rho(T(t,z),P(t))} c_f(t,z) \right) = (c_s(t,z) - 0)$$

Values of the reference internal diffusion coefficients are distinguished for each experiment. The order of magnitude of D_i^R obtained from the optimization is similar to values found by other researchers. Reverchon [4] performed the parameter estimation for the extraction process of sage oil from seeds and reported $D_i^R \approx 6 \cdot 10^{-13}[m^2/s]$. Figure 6a represent the D_i^R as the function of density. As the reference internal diffusion coefficient describes the diffusion inside of a particle, it is independent of external factors such as a fluid velocity around that particle. The reference internal diffusion depends only on local conditions given by temperature and pressure, which defines the physical properties of a stagnant fluid inside of pores of a particle—considering that the reference internal diffusion can be represented as a function of the density of the fluid, which is uniquely defined at a given temperature and pressure in the one-phase region. The linear trend in Figure 6a suggests that D_i^R increases with fluid density.

Similarly to the internal diffusion coefficient, the obtained values of Υ depends only on temperature and pressure, or by uniquely defined physical properties such as density. Figure 6b shows that of Υ grows with density. This can be explained if the solubility increases as the density grows. Shojaie et al. [23], showed that the solubility of carvone (one of the main components of caraway oil) rises together with pressure increase and decreases when temperature increases.

The Figure 6c shows how the internal diffusivity D_i (Equation 15) as a function of the solute concentration in the solid phase at different operating conditions. The higher the density, the higher solubility according to Shojaie et al. [23], which results in higher values of the internal diffusion coefficient and steeper curvature of D_i function.

The axial diffusion coefficient obtained from the optimizer is relatively high compared to the internal diffusion coefficients. The values of D_e^M have a similar order of magnitude as reported in the literature (Reis-Vasco et al. [24]). The axial diffusion can be further analyzed by defining the Peclet number $\left(Pe = \frac{v d_p}{D_e^M} \right)$ and the Reynolds number $\left(Re = \frac{v d_p}{\mu} \right)$, where $d_p = 0.15\,[m]$ is the characteristic dimension defined to be the extractor diameter and μ is the fluid viscosity. The obtained Pecelt numbers are $Pe \gg 1$, which suggests that mass diffusion is negligible and advection dominates mass transport. The experiment was performed in the laminar region and narrow Reynolds number range. Moreover, the volumetric flow-rate was kept constant during all experiments, so the changes in the Reynolds number are related to changes of CO_2 properties at different operating conditions. As the result, the Figure 6d shows a simplified relationship of axial diffusion as a function of density only. The plot show a decrease of the axial diffusion coefficient as the density increase. That behaviour can be
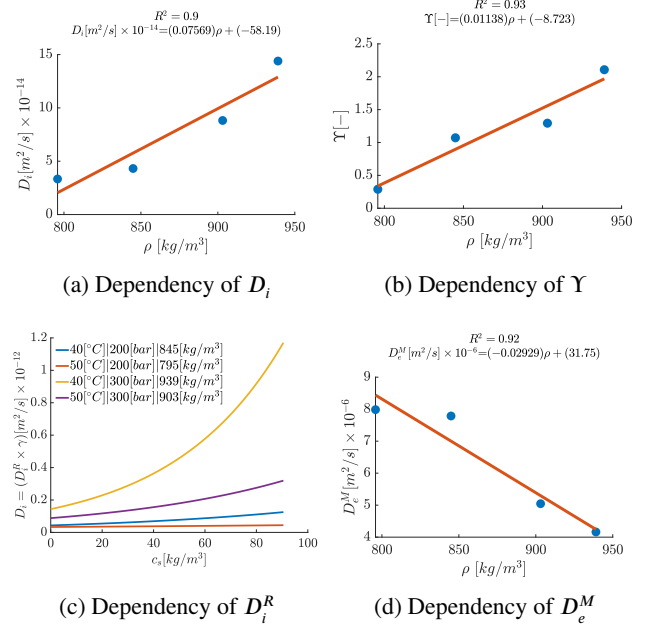

(a) Dependency of D_i (b) Dependency of Υ

(c) Dependency of D_i^R (d) Dependency of D_e^M

Figure 6: Results of parameter estimation

explained by higher resistance of the mass transfer caused by denser fluids.

As the total amount of oil present in the system is unknown, and as such, it has been obtained from the optimizer. Given the dataset and the process model, the optimizer found that the best fit is obtained if the total mass of the oil reaches a lower bound equal to 80 g. The lower bound was estimated by rounding up the biggest value of the collected cumulative amount of the extraction product. As the same raw material was used in all experiments, the same initial amount of solute was assumed for all the cases.

The initial state estimation resulted in values of τ in the range from 0.69 to 0.76. In the equipment used in this experiment, around 25%-30% of the solute was extracted to the fluid phase during the preparation period.

The noise present in each dataset is quantified by the parameter σ^2. It can be observed dataset obtained at 40 °C / 200 bar and 30 °C / 300 bar have similar value of $\sigma^2 \approx 0.07$. The slightly better results were obtained for the experiment at 50 °C / 300 bar when $\sigma^2 \approx 0.05$. The noisiest dataset corresponds to 50 °C / 200 bar when $\sigma^2 \approx 0.12$. All values of σ^2 are relatively low, suggesting the mathematical model can mimic the physical system.

4. Conclusions

This study presented basic aspects regarding the laboratory work for obtaining chamomile extracts using supercritical carbon dioxide at different operating conditions. A first-principle process model was developed based on governing equations. As a result of the literature review, the extraction kinetic model was selected and combined with the general mass balance equations. The values of unknown parameters

in the process model were obtained by parameter estimation. The yield data from the experiments were compared against the yield generated by the model. The IPOPT solver was used to solve the maximum likelihood estimation. The process model was found to have good agreement with experimental yield curves. Later, the parameters found for each experiment were combined to obtain more general relationships. The correlations for diffusion and decay coefficients are presented as a function of fluid density or Reynolds number. It should be noted that obtained correlations have been prepared with a limited amount of data. These correlations can be used to study qualitatively the impact of different operating conditions on the extraction yield by different methods, such as sensitivity analysis. Moreover, the generalized model could be useful in finding the optimal operating conditions with respect to the process economy.

References

[1] Nevena M. Hromis, Vera L. Lazic, Sinisa L. Markov, Zuzana G. Vastag, Senka Z. Popovic, Danijela Z. Suput, Natalija R. Dzinic, Aleksandra S. Velicanski, and Ljiljana M. Popovic. Optimization of chitosan biofilm properties by addition of caraway essential oil and beeswax. Journal of Food Engineering, 158:86–93, aug 2015. doi: 10.1016/j.jfoodeng.2015.01.001.

[2] Ernesto Reverchon, Giorgio Donsi, and Libero Sesti Osseo. Modeling of supercritical fluid extraction from herbaceous matrices. Industrial & Engineering Chemistry Research, 32(11):2721–2726, nov 1993. doi: 10.1021/ie00023a039.

[3] H. Sovova. Rate of the vegetable oil extraction with supercritical co2. modelling of extraction curves. Chemical Engineering Science, 49 (3):409–414, 1994. doi: 10.1016/0009-2509(94)87012-8.

[4] E. Reverchon. Mathematical modeling of supercritical extraction of sage oil. AIChE Journal, 42(6):1765–1771, jun 1996. doi: 10.1002/aic.690420627.

[5] J Elliott. Introductory chemical engineering thermodynamics. Prentice Hall, Upper Saddle River, NJ, 2011. ISBN 9780136068549.

[6] G. G. Simeoni, T. Bryk, F. A. Gorelli, M. Krisch, G. Ruocco, M. Santoro, and T. Scopigno. The widom line as the crossover between liquid-like and gas-like behaviour in supercritical fluids. Nature Physics, 6(7):503–507, jun 2010. doi: 10.1038/nphys1683.

[7] Daniel Banuti. The latent heat of supercritical fluids. Periodica Polytechnica Chemical Engineering, 63(2):270–275, jan 2019. doi: 10.3311/ppch.12871.

[8] W. Sheng, G. J. Chen, and H. C. Lu. Prediction of transport properties of dense gases and liquids by the peng-robinson (PR) equation of state. International Journal of Thermophysics, 10(1):133–144, jan 1989. doi: 10.1007/bf00500714.

[9] Sydney Chapman and T. G. Cowling. The Mathematical Theory of Non-uniform Gases. Cambridge University Press, 1991. ISBN 9780521408448.

[10] A. Fenghour, William A. Wakeham, and V. Vesovic. The viscosity of carbon dioxide. Journal of Physical and Chemical Reference Data, 27 (1):31–44, jan 1998. doi: 10.1063/1.556013.

[11] Arno Laesecke and Chris D. Muzny. Reference correlation for the viscosity of carbon dioxide. Journal of Physical and Chemical Reference Data, 46(1):013107, mar 2017. doi: 10.1063/1.4977429.

[12] M. L. Huber, E. A. Sykioti, M. J. Assael, and R. A. Perkins. Reference correlation of the thermal conductivity of carbon dioxide from the triple point to 1100 k and up to 200 MPa. Journal of Physical and Chemical Reference Data, 45(1):013102, mar 2016. doi: 10.1063/1.4940892.

[13] John D. Anderson. Computational fluid dynamics the basic with applications. McGraw-Hill, 1995. ISBN 9780071132107.

[14] Stefan Schreier. Compressible flow. Wiley, 1982. ISBN 047105691X.

[15] N. R. Bulley, M. Fattori, A. Meisen, and L. Moyls. Supercritical fluid extraction of vegetable oil seeds. Journal of the American Oil Chemists' Society, 61(8):1362–1365, aug 1984. doi: 10.1007/bf02542243.

[16] M. Spiro and M. Kandiah. Extraction of ginger rhizome: partition constants and other equilibrium properties in organic solvents and in supercritical carbon dioxide. International Journal of Food Science & Technology, 25(5):566–575, jun 2007. doi: 10.1111/j.1365-2621.1990.tb01116.x.

[17] Helena Sovova. Broken-and-intact cell model for supercritical fluid extraction: Its origin and limits. The Journal of Supercritical Fluids, 129:3–8, nov 2017. doi: 10.1016/j.supflu.2017.02.014.

[18] Motonobu Goto, Bhupesh C. Roy, and Tsutomu Hirose. Shrinking-core leaching model for supercritical-fluid extraction. The Journal of Supercritical Fluids, 9(2):128–133, jun 1996. doi: 10.1016/s0896-8446(96)90009-1.

[19] Jürgen Gmehling, Michael Kleiber, Bärbel Kolbe, and Jürgen Rarey. Chemical Thermodynamics for Process Simulation. Wiley, mar 2019. doi: 10.1002/9783527809479.

[20] H. Sovova, R. Komers, J. Kucuera, and J. Jezu. Supercritical carbon dioxide extraction of caraway essential oil. Chemical Engineering Science, 49(15):2499–2505, aug 1994. doi: 10.1016/0009-2509(94)e0058-x.

[21] John Mandel. Fitting a straight line to certain types of cumulative data. Journal of the American Statistical Association, 52(280):552–566, dec 1957. doi: 10.1080/01621459.1957.10501413.

[22] Nanci P. Povh, Marcia O.M. Marques, and M.Angela A. Meireles. Supercritical co2 extraction of essential oil and oleoresin from chamomile (chamomilla recutita [l.] rauschert). The Journal of Supercritical Fluids, 21(3):245–256, November 2001. ISSN 0896-8446. doi: 10.1016/s0896-8446(01)00096-1.

[23] G Shojaie, Mohammad Mahdi A. Shirazi, Ali Kargari, and M Shirazi. Solubility prediction of supercritical fluids extraction by equations of state. Journal of Applied Chemical Research, 158:41–59, mar 2010.

[24] E.M.C Reis-Vasco, J.A.P Coelho, A.M.F Palavra, C Marrone, and E Reverchon. Mathematical modelling and simulation of pennyroyal essential oil supercritical extraction. Chemical Engineering Science, 55(15):2917–2922, aug 2000. doi: 10.1016/s0009-2509(99)00561-8.

[25] Ding-Yu Peng and Donald B. Robinson. A new two-constant equation of state. Industrial & Engineering Chemistry Fundamentals, 15(1):59–64, feb 1976. doi: 10.1021/i160057a011.

[26] R. M. Pratt. Thermodynamic properties involving derivatives: Using the peng-robinson equation of state,. Chemical Engineering Education, 35:112–139, 2001. ISSN 0009-2479. URL https://www.tib.eu/de/suchen/id/BLSE%3ARN095457101.

[27] B. G. Kyle. Chemical and process thermodynamics. Prentice Hall PTR, 1999. ISBN 0130874116.

[28] Bruce E. Poling. The properties of gases and liquids. McGraw-Hill, 2001. ISBN 0070116822.

A. Appendix

A.1. Thermodynamic

A.1.1. Equation of state and properties of the fluid phase

A cubic equation of state serves as a mathematical model to describe the behavior of real gases and liquids through a third-degree polynomial equation that correlates the pressure, volume, and temperature of a substance. These equations constitute tools for comprehending the phase behavior, properties, and thermodynamic processes of actual substances, across various engineering and scientific applications. The cubic equation of state take into account deviations from ideal gas behavior, which are particularly important at high pressures and low temperatures, where real gases do not follow assumption of ideal gas.

$$P = \frac{RT}{v_m - b} - \frac{\Phi}{v_m^2 - u v v_m + w b^2} \qquad (32)$$

In this equation, P denotes the pressure of the substance, v_m represents the molar volume of the substance, T stands for the absolute temperature of the substance, u and w are integers that vary from one equation to another, R symbolizes the universal gas constant, and a and b serve as substance-specific parameters known as Van der Waals constants. ω denotes an acentric factor and $\Phi = a\alpha$.

The Van der Waals constants, a and b, constitute empirical values contingent upon the particular substance being modeled. These constants factor in molecular interactions (represented by 'a') and the finite size of gas molecules (indicated by 'b').

Several variations of the cubic equation of state exist each with its own set of parameters and assumptions. Tables 3 show parameters for popular cubic EoS.

EoS	u	w	a	b
van der Waals	0	0	$\frac{27}{64}\frac{R^2 T_c^2}{P_c}$	$\frac{RT_c}{8P_c}$
Redlich and Kwong	1	0	$0.42748\frac{R^2 T_c^{2.5}}{P_c}$	$\frac{0.08664 RT_c}{P_c}$
Soave	1	0	$0.42748\frac{R^2 T_c^2}{P_c}$	$\frac{0.08664 RT_c}{P_c}$
Peng and Robinson [25]	2	-1	$0.45724\frac{R^2 T_c^2}{P_c}$	$\frac{0.07780 T_c}{P_c}$

Table 3: Parameters for Popular Cubic EoS

EoS	α	$f(\omega)$
van der Waals	-	-
Redlich and Kwong	$\frac{1}{\sqrt{T_r}}$	-
Soave	$\left[1 + f(\omega)\left(1 - \sqrt{T_r}\right)\right]^2$	$0.48+1.574\omega-0.176\omega^2$
Peng and Robinson [25]	$\left[1 + f(\omega)\left(1 - \sqrt{T_r}\right)\right]^2$	$0.37464+1.54226\omega-0.26992\omega^2$

Table 4: Parameters for Popular Cubic EoS

The general cubic equation of state can be represented as a polynomial, as indicated in Equation 33. In a one-phase region, the fluid is characterized by a single real root, corresponding to the gas, liquid, or supercritical phase. In the two-phase region, a gas-liquid mixture exists, and two roots are identified. The larger root corresponds to the gas phase, while the smaller root pertains to the liquid phase.

$$Z^3 - (1 + B - uB)Z^2 + (A + wB^2 - uB - uB^2)Z - AB - wB^2 - wB^3 = 0 \qquad (33)$$

where $A = \frac{\Phi P}{R^2 T^2}$ and $B = \frac{bP}{RT}$.

If the Peng-Robinson equation of state [[25]] is used, the polynomial equation becomes

$$Z^3 - (1 - B)Z^2 + (A - 2B - 3B^2)Z - (AB - B^2 - B^3) = 0 \qquad (34)$$

For an ideal gas, the compressibility factor is defined as $Z = 1$, but to describe real-life physical phenomena, the deviation of Z needs to be consider. The value of Z typically increases with pressure and decreases with temperature. At elevated pressures, molecules collide more frequently, allowing repulsive forces between molecules to influence the molar volume of the real gas (v_m) to surpass that of the corresponding ideal gas $\left((v_m)_{ideal\ gas} = \frac{RT}{P}\right)$, resulting in Z exceeding one. At lower pressures, molecules move freely, with attractive forces predominating, leading to $Z < 1$.

Numerical methods such as Newton-Raphson can be used to solve the polynomial equation to obtain the compressibility $Z(T(t, z), P(t))$ at given temperature and pressure. Alternatively, the closed form solution can by obtained by Cardano formula. Details regarding the Cardano formula can be found in Appendix A.3.

A.1.2. Density of the fluid phase

The density of the fluid can be calculated from the real gas equation $\rho = \frac{P}{RTZ}\frac{1}{m_{CO2}}$. The local temperature can be obtain from the time evolution of governing equations, the pressure is consider to be constant along the system to be a know at any time. The local compressibility factor can be also computed if the local temperature and pressure are know. To obtain the density in terms of mass, molar mass of the solvent is taken into account.

A.1.3. Heat capacity of the fluid phase

The specific heat C_p^F can be calculated from the equation of state, under the assumption that the fluid phase consists of pure carbon dioxide and that the specific heat of real fluids can be calculated from an ideal contribution plus a residual term Pratt [26]:

$$C_v = C_v^{id} + C_v^R \qquad (35)$$
$$C_p = C_p^{id} + C_p^R \qquad (36)$$

The ideal-gas contribution is found using heat-capacity data applicable to gases at very low pressures, which are available in many thermodynamics textbooks in the polynomial form, such as $C_p^{id}(T) = A + BT + CT^2 + DT^3$.

where the coefficients of the expansion are $C_{P0} = 22.26$, $C_{P1} = 5.981 \times 10^{-2}$, $C_{P2} = -3.501 \times 10^{-5}$, and $C_{P3} = 7.469 \times 10^{-9}$, as given by Kyle [27].

The residual component of the specific heat can obtained from general relation between C_v and C_p as given by Poling [28].

$$C_p^R = C_v^R + T\left(\frac{\partial P}{\partial T}\right)_{v_m}\left(\frac{\partial v_m}{\partial T}\right)_P - R \qquad (37)$$

The effects of pressure and temperature for liquids are not great, but both C_p and C_v diverge at the critical point of a pure fluid. In the neighborhood of the critical, $\left(\frac{\partial P}{\partial v_m}\right)_T$ approaches zero, so C_p increases much faster than C_v. At both high and low densities, the differences are small, but for T_r near unity, they increase rapidly as the critical density is approached. At fixed density in this region, C_p actually decreases as T increases.

The term $\left(\frac{\partial P}{\partial T}\right)_{v_m}$ can be obtain by direct differentiation of P-R EoS

$$\left(\frac{\partial P}{\partial T}\right)_{v_m} = \frac{R}{v_m - b} - \frac{\frac{d\Phi}{dT}}{\left[v_m(v_m + b) + b(v_m - b)\right]^2} \tag{38}$$

where $\left(\frac{\partial \Phi}{\partial T}\right)_{v_m} = \frac{-f(\omega)a}{\sqrt{TT_c}(1+f(\omega)(1-\sqrt{T/T_c}))}$

The term $\left(\frac{\partial v_m}{\partial T}\right)_P = \frac{R}{P}\left(T\left(\frac{\partial Z}{\partial T}\right)_P + Z\right)$

The term $\left(\frac{\partial Z}{\partial T}\right)_P$ can be defined as below

$$\left(\frac{\partial Z}{\partial T}\right)_P = \frac{\left(\frac{\partial A}{\partial T}\right)_P(B - Z) + \left(\frac{\partial B}{\partial T}\right)_P\left(6BZ + 2Z - 3B^2 - 2B + A - Z^2\right)}{3Z^2 + 2(B-1)Z + (A - 2B - 3B^2)} \tag{39}$$

$$\left(\frac{\partial A}{\partial T}\right)_P = (P/(RT)^2)(\frac{d\Phi}{dT} - 2a/T) \tag{40}$$

$$\left(\frac{\partial B}{\partial T}\right)_P = -bP/(RT^2) \tag{41}$$

The first component of Equation 37 from definition of $C_v = \left(\frac{\partial U^R}{\partial T}\right)_{v_m}$, where U^R represents internal energy. In case of Pen-Robinson U^R equals to

$$U^R = \frac{T\frac{d^2\Phi}{dT^2}}{b\sqrt{8}} \ln\left(\frac{Z + B\left(1 + \sqrt{2}\right)}{Z + B\left(1 - \sqrt{2}\right)}\right) \tag{42}$$

As given by Pratt [26], for Peng-Robinson EoS the term $\frac{d^2\Phi}{dT^2}$ is defined as follow

$$\frac{d^2\Phi}{dT^2} = \frac{af(\omega)\sqrt{\frac{T_c}{T}}(1 + f(\omega))}{2TT_c} \tag{43}$$

A.1.4. Departure functions for enthalpy calculations

In thermodynamics, a departure function is a concept used to calculate the difference between a real fluid's thermodynamic properties (enthalpy, entropy, or internal energy) and those of an ideal gas, given a specific temperature and pressure. These functions are used to calculate extensive properties, which are properties computed as a difference between two states.

To evaluate the enthalpy change between two points, $h(V_1, T_1)$ and $h(V_2, T_2)$, the enthalpy departure function between the initial volume V_1 and infinite volume at temperature T_1 is calculated. Then it is added to that the ideal gas enthalpy change due to the temperature change from T_1 to T_2, and finally subtract the departure function value between the final volume V_2 and infinite volume.

Departure functions are computed by integrating a function that depends on an equation of state and its derivative. The general form of the enthalpy equation is given by:

$$\frac{h^{id} - h}{RT} = \int_{v_m}^{\infty} \left(T\left(\frac{\partial Z}{\partial T}\right)_{v_m}\right)\frac{dv_m}{v_m} + 1 - Z \tag{44}$$

Here, h^{id} represents the enthalpy of an ideal gas, h is the enthalpy of a real fluid, R is the universal gas constant, T is temperature, v_m is the molar volume, and Z is the compressibility factor.

The integral in the equation is evaluated over the range of molar volumes from v_m to infinity. The integral includes a term that depends on the derivative of the compressibility factor with respect to temperature, evaluated at the molar volume v_m. Finally, the term $1 - Z$ is added to account for the deviation of the fluid's properties from an ideal state.

The Peng–Robinson EoS relates the three interdependent state properties pressure P, temperature T, and molar volume v_m. From the state properties (P, v_m, T), one may compute the departure function for enthalpy per mole (denoted h) as presented by Gmehling et al. [19] or Elliott [5]:

$$h - h^{id} = RT_c\left[T_r(Z - 1) - 2.078(1 + \kappa)\sqrt{\alpha}\ln\left(\frac{Z + 2.414B}{Z - 0.414B}\right)\right] \tag{45}$$

A.2. Governing equations
A.2.1. Mass continuity

Following the work of Anderson [13], the governing equations for compressible fluid with non-uniform cross-section can be obtained. Let's assume that any properties of the flow are uniform across any given cross-section of an extractor. The variation of the cross-section might result from the partial filling of an extractor or its irregular shape. In reality, such a flow is two-dimensional because the area changes as a function of z, and there is a flow-field variation in both directions. The assumption of quasi-one-dimensional flow dictates that the flow properties are a function of z only. The integral form of the continuity equation is:

$$\frac{\partial}{\partial t}\iiint_{V_f} \rho_f dV_f + \iint_S \rho_f \mathbf{V} \cdot d\mathbf{S} = 0 \tag{46}$$

We apply this equation to the shaded control volume shown in Figure 7.
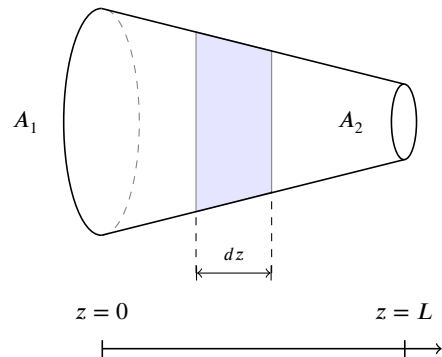

Figure 7: Control volume for deriving the partial differential equation for unsteady, quasi-one-dimensional flow

On the left side of the control volume, consistent with the quasi-one-dimensional assumptions, the density, velocity, pressure, and internal energy denoted by ρ_f, v, P, and e, respectively, are uniform over the area A. Similarly, on the right side of the control volume, the density, velocity,

pressure, and internal energy $\rho_f + d\rho_f$, $v + dv$, $P + dP$, and $e + de$, respectively, are uniform over the area available for fluid phase $A_f + dA_f$. Applied to the control volume in Figure 7, the volume integral in Equation 46 becomes, in the limit as dz becomes very small,

$$\frac{\partial}{\partial t} \iiint_{\mathcal{V}_f} \rho_f d\mathcal{V}_f = \frac{\partial}{\partial t}\left(\rho_f A_f dz\right) \tag{47}$$

where $A\,dz$ is the volume of the control volume in the limit of dz becoming vanishingly small. The surface integral in Equation 46 becomes

$$\iint_S \rho_f \mathbf{V} \cdot \mathbf{dS} = -\rho_f v A_f + (\rho_f + d\rho_f)(v + dv)(A_f + dA_f) \tag{48}$$

The minus sign on the leading term on the right-hand side is due to the vectors $\mathbf{V}$ and $\mathbf{dS}$ pointing in opposite directions over the left of the control volume, and hence the dot product is negative. Expanding the triple product term

$$\iint_S \rho_f \mathbf{V} \cdot \mathbf{dS} = -\rho_f v A_f + \rho_f v A_f + \rho_f v dA_f + \rho_f A_f dv$$
$$+ \rho_f dv dA_f + v A_f d\rho_f + v d\rho_f dA + A_f d\rho_f dv + d\rho_f dv dA_f \tag{49}$$

In the limit as dz becomes very small, the terms involving products of the differential in Equation 49, such as $\rho_f dv dA_f$, $d\rho_f dv dA_f$, go to zero much faster than those terms involving only one differential. Hence, all terms involving products of differentials can be dropped, yielding in the limit as dz becomes very small

$$\iint_S \rho_f \mathbf{V} \cdot \mathbf{dS} = \rho_f v dA_f + \rho_f A_f dv + v A_f d\rho_f \tag{50}$$

Substituting Eqs. 47 and 50 into 46, we have

$$\frac{\partial\left(\rho_f A_f\right)}{\partial t} + \frac{\partial\left(\rho_f A_f v\right)}{\partial z} = 0 \tag{51}$$

The above partial differential equation form of the continuity equation is suitable for unsteady, quasi-one-dimensional flow. The $A_f(z)$ is an arbitrary function that describes a change in the extractor's cross-section and can be defined as $A_f(z) = \mathbf{A}\phi(z)$, where ϕ is the bed porosity and $\mathbf{A}$ is the cross-section of an empty extractor.

$$\frac{\partial\left(\rho_f \mathbf{A}\phi(z)\right)}{\partial t} + \frac{\partial\left(\rho_f \mathbf{A}\phi(z)v\right)}{\partial z} = 0 \tag{52}$$

The equation can be simplified by canceling out a constant $\mathbf{A}$

$$\frac{\partial\left(\rho_f \phi(z)\right)}{\partial t} + \frac{\partial\left(\rho_f \phi(z)v\right)}{\partial z} = 0 \tag{53}$$

If so-called superficial velocity is defined as $u = \phi v$, the mass continuity becomes

$$\frac{\partial\left(\rho_f \phi(z)\right)}{\partial t} + \frac{\partial\left(\rho_f u\right)}{\partial z} = 0 \tag{54}$$

A.2.2. Transport of a species

The transport of a solute, can be described by an analogous equation to the Equation 46 with additional terms on the right-hand side. The first term on the right-hand side describes diffusional movement of species and is based on the Fick's law $\left(J_{diff} = D_e^M \frac{\partial c_f}{\partial z}\right)$. The other term corresponds

to the mass transfer between solid and fluid phases, which is treated as a source term.

$$\frac{\partial}{\partial t} \iiint_{\mathcal{V}_f} c_f d\mathcal{V}_f + \iint_S c_f \mathbf{V} \cdot \mathbf{dS} = \iint_S J_{diff} \cdot \mathbf{n}\, dS + \frac{\partial}{\partial t} \iiint_{\mathcal{V}_s} c_s d\mathcal{V}_s \tag{55}$$

Similarly to the continuity equation, in the limit as dz becomes very small

$$\frac{\partial}{\partial t} \iiint_{\mathcal{V}_f} c_f d\mathcal{V}_f = \frac{\partial}{\partial t}\left(c_f A_f dz\right) \tag{56}$$

$$\frac{\partial}{\partial t} \iiint_{\mathcal{V}_s} c_s d\mathcal{V}_s = \frac{\partial}{\partial t}\left(c_s A_s dz\right) \tag{57}$$

The surface integrals in the limit of dz become

$$\iint_S c_f \mathbf{V} \cdot \mathbf{dS} = c_f v dA_f + c_f A_f dv + v A_f dc_f \tag{58}$$

From the Divergence theorem in multi-variable calculus, we have

$$\iint_S J_{diff} \cdot \mathbf{n}\, dS = \iiint_{\mathcal{V}_f} \nabla J_{diff} dv_f = \nabla \iiint_{\mathcal{V}_f} J_{diff} dv_f = \nabla\left(J_{diff} A_f dz\right) \tag{59}$$

By substituting the equations derived above into Equation 55 we obtain

$$\frac{\partial\left(c_f A_f\right)}{\partial t} + \frac{\partial\left(c_f A_f v\right)}{\partial z} = \frac{\partial\left(c_s A_s\right)}{\partial t} + \frac{\partial\left(J_{diff} A_f\right)}{\partial z} \tag{60}$$

By defining $A_f = A \cdot \phi$, $A_s = A \cdot (1 - \phi)$ and $u = V \cdot \phi$, and assuming that A is constant, the above equation becomes

$$\frac{\partial\left(c_f \phi\right)}{\partial t} + \frac{\partial\left(c_f u\right)}{\partial z} = \frac{\partial\left(c_s(1-\phi)\right)}{\partial t} + \frac{\partial\left(J_{diff} \phi\right)}{\partial z} \tag{61}$$

By assuming that $\frac{\partial \phi}{\partial t} = 0$ and expanding J_{diff}, we get

$$\frac{\partial c_f}{\partial t} + \frac{1}{\phi}\frac{\partial\left(c_f u\right)}{\partial z} = \frac{(1-\phi)}{\phi}\frac{\partial c_s}{\partial t} + \frac{1}{\phi}\frac{\partial}{\partial z}\left(D_e^M \frac{\partial c_f}{\partial z}\right) \tag{62}$$

The equation can be further simplified if $\frac{\partial u}{\partial z} = \frac{\partial \phi}{\partial z} = D_e^M = 0$, which corresponds to the assumptions of constant velocity along the bed(which might be a case of isothermal and low-Mach number flow), constant porosity(which comes from the assumption of constant area for both solid and fluid phase) and no radial diffusion.

$$\frac{\partial c_f}{\partial t} + \frac{u}{\phi}\frac{\partial c_f}{\partial z} = \frac{1-\phi}{\phi}\frac{\partial c_s}{\partial t} \tag{63}$$

The Equation 63 is equivalent to the equation presented by Reverchon [4].

A.2.3. Momentum conservation

Similarly to mass conservation, momentum conservation is derived for inviscid fluid with no body forces

$$\frac{\partial}{\partial t} \iiint_{\mathcal{V}_f} \left(\rho_f v_z\right) d\mathcal{V}_f + \iint_S \left(\rho_f v_z \mathbf{V}\right) \mathbf{dS} = \iint_S (P dS)_z \tag{64}$$

where V_z is the z component of the velocity.

We the momentum conservation to the shaded control volume in Figure 7, the integrals on the left side are evaluated in the same manner as discussed above in the regard to the continuity equation. That is,
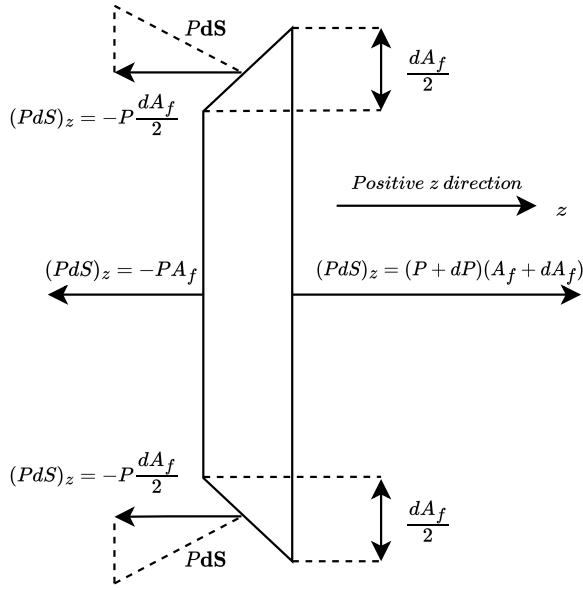
Figure 8: The forces in the z direction acting on the control volume

$$\frac{\partial}{\partial t}\iiint_{\mathcal{V}_f}\left(\rho_f v_z\right)d\mathcal{V}_f = \frac{\partial}{\partial t}\left(\rho_f v A_f dz\right) \tag{65}$$

equation

and

$$\iint_S \left(\rho_f v_z \mathbf{V}\right)dS = -\rho_f v^2 + \left(\rho_f + d\rho_f\right)(v+dv)^2\left(A+dA\right) \tag{66}$$

The evaluation of the pressure force term on the right side of Equation 64 can be understood based on the Figure 8. Here, the z components of the vector PdS are shown on all four sides of the control volume. Remember that $\mathbf{dS}$ is assumed to point away from the control volume; hence any z component $(PdS)_z$ that acts toward the left (in the negative z direction) is a negative quantity. Any z component that acts toward the right (in the positive z direction) is a positive quantity. Also note that the z component of PdS acting on the top and the bottom inclined faces of the control volume in Figure 8 can be expressed as the pressure P acting on the component of the inclined is projected perpendicular to the z direction, $dA_f/2$; hence, the contribution of each inclined face (top or bottom) to the pressure integral in Equation 64 is $-P(dA_f/2)$. All together, the right-hand side of Equation 64 is expressed as follows:

$$\iint (PdS)_z = -PA_f + (P+dP)(A+dA_f) - 2P\frac{dA_f}{2} \tag{67}$$

Substituting Eqs. 65 to 67 into Equation 64, we have

$$\frac{\partial}{\partial t}\left(\rho_f v A_f dz\right) - \rho_f v^2 A_f + (\rho_f + d\rho_f)(v+dv)^2(A_f + dA_f)$$
$$= PA_f - (P+dP)(A+dA_f) + PdA_f \tag{68}$$

Canceling like terms and ignoring products of differentials, the equation above becomes in the limit dz becoming very small

$$\frac{\partial}{\partial t}\left(\rho_f v A_f dz\right) + d\left(\rho_f v^2 A_f\right) = -AdP \tag{69}$$

Dividing the above equation by dz and taking the limit as dz goes to zero, we obtain

$$\frac{\partial\left(\rho_f v A_f\right)}{\partial t} + \frac{\partial\left(\rho_f v^2 A_f\right)}{\partial z} = -A_f\frac{\partial P}{\partial z} \tag{70}$$

The Equation 70 can be expanded further by assuming that $A_f = \mathbf{A}\phi$

$$\frac{\partial\left(\rho_f v \mathbf{A}\phi\right)}{\partial t} + \frac{\partial\left(\rho_f v^2 \mathbf{A}\phi\right)}{\partial z} = -\mathbf{A}\phi\frac{\partial P}{\partial t} \tag{71}$$

The equation can be further simplified by assuming that the cross-section of an extractor $\mathbf{A}$ is constant and cancel out

$$\frac{\partial\left(\rho_f v \phi\right)}{\partial t} + \frac{\partial\left(\rho_f v^2 \phi\right)}{\partial z} = -\phi\frac{\partial P}{\partial t} \tag{72}$$

If the superficial velocity $u = \phi V$ is introduced, then the momentum conservation becomes

$$\frac{\partial\left(\rho_f u\right)}{\partial z} + \frac{\partial\left(\rho_f u^2/\phi\right)}{\partial z} = -\phi\frac{\partial P}{\partial z} \tag{73}$$

Equation 70 represents the conservative form of the momentum equation for the quasi-one-dimensional flow. The equivalent non-conservative form can be obtained by multiplying the continuity equation by v and subtracting it from Equation 70

$$\frac{\partial\left(\rho_f v A_f\right)}{\partial t} - V\frac{\partial\left(\rho_f A_f\right)}{\partial t} + \frac{\left(\rho_f v^2 A_f\right)}{\partial z} - V\frac{\left(\rho_f v A_f\right)}{\partial z} = -A_f\frac{\partial P}{\partial z} \tag{74}$$

Expanding the derivatives on the left-hand side of the above equation and canceling like terms, gives

$$\rho_f A_f\frac{\partial v}{\partial t} + \rho_f A_f v\frac{\partial v}{\partial z} = -A_f\frac{\partial P}{\partial z} \tag{75}$$

Dividing the above equation by A_f the non-conservative form of the momentum can be obtained

$$\rho_f\frac{\partial v}{\partial t} + \rho_f v\frac{\partial v}{\partial z} = -\frac{\partial P}{\partial z} \tag{76}$$

The Equation 76 is stylistically the same as the general momentum conservation for one-dimensional flow with no-body forces. The momentum equation can be expressed in terms of superficial velocity $u = v\phi$.

$$\rho_f\frac{\partial\left(u/\phi\right)}{\partial t} + \rho_f\frac{u}{\phi}\frac{\partial\left(u/\phi\right)}{\partial z} = -\frac{\partial P}{\partial z} \tag{77}$$

By expanding all the terms of the equation above, we get

$$\frac{\rho_f}{\phi}\frac{\partial u}{\partial t} + \rho_f u\frac{\partial\phi^{-1}}{\partial t} + \rho_f\frac{u}{\phi}\frac{1}{\phi}\frac{\partial u}{\partial z} + \rho_f\frac{u}{\phi}u\frac{\partial\phi^{-1}}{\partial z} = -\frac{\partial P}{\partial z} \tag{78}$$

If the bed is not compressible and doesn't change its properties during the batch, then $\frac{\partial\phi}{\partial t} = 0$

$$\frac{\rho_f}{\phi}\left(\frac{\partial u}{\partial t} + \frac{u}{\phi}\frac{\partial u}{\partial z} + u^2\frac{\partial\phi^{-1}}{\partial z}\right) = -\frac{\partial P}{\partial z} \tag{79}$$

If the porosity is constant along an extractor, then the momentum conservation equation becomes

$$\frac{\rho_f}{\phi}\left(\frac{\partial u}{\partial t} + \frac{u}{\phi}\frac{\partial u}{\partial z}\right) = -\frac{\partial P}{\partial z} \tag{80}$$

The Equation 80 represents the non-conservative form of the momentum equation for quasi-one-dimensional flow with no body forces and constant porosity.

A.2.4. Energy conservation

Let's consider the integral form of the energy equation for adiabatic flow with no body forces and no viscous effects

$$\frac{\partial}{\partial} \iiint_{\mathcal{V}_f} \rho_f \left(e_f + \frac{v^2}{2} \right) d\mathcal{V}_f + \iint_S \rho_f \left(e_f + \frac{v^2}{2} \right) \mathbf{V} \cdot \mathbf{dS} = - \iint_S (PV) \cdot \mathbf{dS}$$

(81)

Applied to the shaded control volume in Figure 7, and keeping in mind the pressure forces shown in Figure 8, Equation 81 becomes

$$\frac{\partial}{\partial t} \left[\rho_f \left(e_f + \frac{v^2}{2} \right) A_f dz \right] - \rho_f \left(e_f + \frac{v^2}{2} \right) v A_f$$
$$+ (\rho_f + d\rho_f) \left[e_f + de_f + \frac{(v+dv)^2}{2} \right] (V + dV) \left(A_f + dA_f \right)$$
$$= - \left[-PvA_f + (P + dP)(v + dv)\left(A_f + dA_f \right) - 2 \left(Pv \frac{dA_f}{2} \right) \right]$$

(82)

Neglecting products of differential and canceling like terms, the above equation becomes

$$\frac{\partial}{\partial t} \left[\rho_f \left(e_f + \frac{v^2}{2} \right) A_f dz \right] + d\left(\rho_f r_f A_f \right) + \frac{\left(\rho_f v^3 A_f \right)}{2} = -d\left(PA_f v \right)$$

(83)

or

$$\frac{\partial}{\partial t} \left[\rho_f \left(e_f + \frac{v^2}{2} \right) A_f dz \right] + d\left[\rho_f \left(e_f \frac{v^2}{2} \right) v A_f \right] = -d\left(PA_f v \right)$$

(84)

Taking the limit as dz approaches zero, the equation above becomes the following partial differential equation

$$\frac{\partial \left[\rho_f \left(e_f + v^2/2 \right) A \right]}{\partial t} + \frac{\partial \rho_f \left(e_f + v^2/2 \right) v A_f}{\partial z} = - \frac{\partial \left(PA_f v \right)}{\partial z}$$

(85)

Equation 85 is the conservation form of the energy expressed in terms of the total energy $e + v^2/2$, appropriate for unsteady, quasi-one-dimensional flow. The energy equation can be expressed in terms of internal energy if Equation 70 is multiplicated by v and then subtracted from Equation 85

$$\frac{\partial \left(\rho_f e_f A_f \right)}{\partial t} + \frac{\partial \left(\rho_f e_f v A_f \right)}{\partial z} = -P \frac{\partial A_f v}{\partial z}$$

(86)

The equation above is the conservation form of the energy equation expressed in terms of internal energy e_f suitable for quasi-one-dimensional flow. The non-conservative for is then obtained by multiplying the continuity equation 51, by e_f and substructing it from 86, yielding

$$\rho_f A_f \frac{\partial e_f}{\partial t} + \rho_f A_f v \frac{\partial e_f}{\partial z} = -P \frac{\partial (A_f v)}{\partial z}$$

(87)

Expanding the right-hand side and dividing by A_f, the above equation becomes

$$\rho_f \frac{\partial e_f}{\partial t} + \rho_f v \frac{\partial e_f}{\partial z} = -P \frac{v}{A_f} \frac{\partial A_f}{\partial z}$$

(88)

or

$$\rho_f \frac{\partial e_f}{\partial t} + \rho_f v \frac{\partial e_f}{\partial z} = -P \frac{\partial v}{\partial z} - PV \frac{\partial (\ln A_f)}{\partial z}$$

(89)

Equation 89 is the non-conservative form of the energy equation expressed in terms of internal energy, appropriate to unsteady quasi-one-dimensional flow. The reason for obtaining the energy equation in the form of Equation 89 is that, for a calorically perfect gas, it leads directly to a form of the energy equation in terms of temperature T.

A.3. Cardano's Formula

Following the work of Gmehling et al. [19], a cubic equation of state can be written a following form

$$Z^3 + UZ^2 + SZ + T = 0$$

(90)

with Z as the compressibility factor. Using Cardano's formula, this type of equation can be solved analytically. With the abbreviations

$$P = \frac{3S - U^2}{3} \qquad Q = \frac{2U^3}{27} - \frac{US}{3} + T$$

the discriminant can be determined to be

$$D = \left(\frac{P}{3} \right)^3 + \left(\frac{Q}{2} \right)^2$$

(91)

For $D > 0$, the equation of state has one real solution:

$$Z = \left[\sqrt{D} - \frac{Q}{2} \right]^{1/3} - \frac{P}{3 \left[\sqrt{D} - \frac{Q}{2} \right]^{1/3}} - \frac{U}{3}$$

(92)

For $D < 0$, there are three real solutions. With the abbreviations

$$\Theta = \sqrt{-\frac{P^3}{27}} \qquad \Phi = \arccos\left(\frac{-Q}{2\Theta} \right)$$

they can be written as

$$Z_1 = 2\Theta^{(1/3)} \cos\left(\frac{\Phi}{3} \right) - \frac{U}{3}$$

(93)

$$Z_2 = 2\Theta^{(1/3)} \cos\left(\frac{\Phi}{3} + \frac{2\pi}{3} \right) - \frac{U}{3}$$

(94)

$$Z_3 = 2\Theta^{(1/3)} \cos\left(\frac{\Phi}{3} + \frac{4\pi}{3} \right) - \frac{U}{3}$$

(95)

The largest and the smallest of the three values correspond to the vapor and to the liquid solutions, respectively. The middle one has no physical meaning.

A.4. Maximum likelihood

Maximum likelihood estimation (MLE) is a statistical method used to estimate the parameters of a probability distribution based on observed data. The MLE works by finding the values of the parameters that maximize the likelihood function, which is the probability of observing the given data for a given set of parameter values. The MLE has desirable properties such as asymptotic efficiency and normality. Although the MLE has often been associated with the normal distribution for mathematical convenience, it can be applied to a wide range of probability distributions.

To find the maximum likelihood estimates, we maximize the joint probability density function, or likelihood function, denoted as $p(\theta|y(t_1), y(t_2), ..., y(t_n))$, where θ represents the parameters and $y(t_1), y(t_2), ..., y(t_n)$ represent the observed data. The conditions at the maximum can be refined by incorporating prior information. The posterior probability density function $p(\theta|y)$ can be expressed as the ratio of two probability densities using the continuous variable analogue of Bayes' theorem . In such a case the posteriori distribution is given by Equation 96.

$$p\left(\theta|y(t_n),...,y(t_1)\right) = \frac{p\left(\theta,y(t_n),...,y(t_1)\right)}{p\left(y(t_n),...,y(t_1)\right)} \tag{96}$$

The numerator of the right-hand side od Equation 96 becomes

$$p\left(\theta,y(t_n),...,y(t_1)\right) = p\left(y(t_n)|\theta,y(t_{n-1}),...,y(t_1)\right) \\ \cdot p\left(\theta,y(t_{n-1}),...,y(t_1)\right) \tag{97}$$

These operations can be continued repetitively until we get

$$p\left(\theta,y(t_n),...,y(t_1)\right) = p(\theta)\prod_{i=1}^{n}p\left(y(t_i)|\theta,y(t_{i-1}),...,y(t_1)\right) \tag{98}$$

Examination of Equation 28 shows that $dY(t_i)/dt$ depends only on t_i, θ and $\epsilon(t_i)$ and is not conditioned by any previous measurement. Consequently, we can write

$$p\left(y(t_i)|\theta,y(t_{i-1}),...,y(t_1)\right) = p\left(y(t_i)|\theta\right) \tag{99}$$

provided Equation 28 is observed as a constraint. The desired joint conditional probability function is thus

$$p\left(\theta|y(t_n),...,y(t_1)\right) = \frac{p(\theta)\prod_{i=1}^{n}p\left(y(t_i)|\theta\right)}{p\left(y(t_n),...,y(t_1)\right)} \tag{100}$$

We can get rid of the evidence term $p\left(y(t_n),...,y(t_1)\right)$ because it's constant with respect to the maximization. Moreover, if we are lacking a prior distribution over the quantity we want to estimate, then $p(\theta)$ can be omitted. In such a case:

$$p\left(\theta|y(t_n),...,y(t_1)\right) = \prod_{i=1}^{n}p\left(y(t_i)|\theta\right) = \prod_{i=1}^{n}L\left(\theta|y(t_i)\right) \tag{101}$$

The likelihood function $L\left(\theta|y\right)$ for the parameters based on several observations is the product of the individual functions if the observations are independent.

$$L\left(\theta|y(t_n),...,y(t_1)\right) = \prod_{i=1}^{n}L\left(\theta|y(t_i)\right) \\ = p\left(y(t_1)|\theta\right)p\left(y(t_2)|\theta\right)...p\left(y(t_n)|\theta\right) \tag{102}$$

In choosing as estimates of θ the values that maximize L for the given values $\left(y(t_i)\right)$, it turns out that it is more convenient to work with the $\ln L$ than with L itself:

$$\ln L = \ln p\left(y(t_1)|\theta\right)+\ln p\left(y(t_2)|\theta\right)+...+\ln p\left(y(t_n)|\theta\right) = \sum_{i=1}^{n}\ln p\left(y(t_i);\theta\right) \tag{103}$$

By assuming that the conditional distribution of $\bar{Y}_i$, given y_i, is normal, then we form the likelihood function based on the probability density:

$$p\left(\theta,\sigma|y(t_n),...,y(t_1)\right) = \prod_{i=1}^{n}\frac{1}{\sqrt{2\pi}\sigma}\exp\left[\frac{1}{2\sigma}\left(Y(t_i)-y(\theta,t_i)\right)^2\right]$$

$$L\left(\theta,\sigma|y(t_n),...,y(t_1)\right) = \prod_{i=1}^{n}\frac{1}{\sqrt{2\pi}\sigma}\exp\left[\frac{1}{2\sigma}\left(Y(t_i)-y(\theta,t_i)\right)^2\right] \tag{104}$$

where σ is the variance

By taking the natural logarithm of the Equation 104, the final form of the objective function can be obtained:

$$\ln L = -\frac{n}{2}\left(\ln\sqrt{2\pi}+\ln\sigma^2\right)-\frac{\sum_{i=1}^{n}\left[Y(t_i)-y(\theta,t_i)\right]^2}{2\sigma^2} \tag{105}$$